Cement and Concrete Research 39 (2009) 763–772

Contents lists available at ScienceDirect

Cement and Concrete Research

journal homepage: http://ees.elsevier.com/CEMCON/default.asp

Modelling and simulations of the chemo–mechanical behaviour of leached cement-based materials
Leaching process and induced loss of stiffness

E. Stora [a,b,*], B. Bary [a], Q.-C. He [b], E. Deville [c], P. Montarnal [c]

[a] Atomic Energy Commission, CEA, DEN, DPC, SCCME, Laboratoire d'Etude du Comportement des Bétons et des Argiles, 91191 Gif sur Yvette, France
[b] Université Paris-Est, Laboratoire de Modélisation et Simulation Multiéchelle, FRE3160 CNRS, 5 boulevard Descartes, 77454 Marne-la-Vallée Cedex 2, France
[c] CEA, DEN, DM2S, SFME, MTMS, 91191 Gif sur Yvette, France

ARTICLE INFO

Article history:
Received 25 February 2008
Accepted 26 May 2009

Keywords:
Chemo–mechanical degradations
Leaching
C. elastic moduli
C. micromechanics
D. cement paste
E. modelling

ABSTRACT

The present paper aims at modelling the decalcification process in cement-based materials and its impact on the material stiffness, which represents a serious matter in terms of long-term durability. The resistance of cementitious materials to this chemical alteration is strongly conditioned by their mineral composition and porosity. For this purpose, a multi-scale homogenization approach (Stora et al., *Trans. Por. Med*. 73, 3, 2008) is implemented in the numerical platform ALLIANCES (P. Montarnal, C. Mügler, J. Colin, M. Descotes, A. Dimier, E. Jacquot, Presentation and use of a reactive transport code in porous media, Phys. Chem. Earth 32, 2007) to estimate from these data the elastic and diffusive properties of cement-based materials. The association of this homogenization model and of the integration platform, which can couple different numerical codes, then allows for evaluating the evolution of the mineral composition and of the diffusive and mechanical properties of a concrete material during chemical deterioration processes. Simulations of pure water leaching of hydrated cement pastes are performed and the consequences of this decalcification on the material's residual elastic behaviour are estimated. The numerical results are confronted with available experimental data and analyzed. The simulations of the non-linear mechanical behaviour of leached cementitious materials taking into account interactions between damage and leaching is not reported here for conciseness but can be found in another document (Stora, Modelling and simulations of the chemo–mechanical behaviour of leached cement-based materials. PhD Dissertation, univ. of Paris-Est 2008).

1. Introduction

Concrete facilities that are in contact with ground water, such as dams or nuclear waste disposals, are exposed to decalcification reactions. The leaching of cement-based materials by pure water or ionic solutions has a strong impact on their microstructure (e.g. [1,2]) because of the dissolution of hydrated phases such as portlandite (CH) or aluminates (AF). These dissolution reactions originated by ionic migration between the interstitial solution and ground water affects the mechanical and transport properties of these building materials (e.g. [3,4]). Despite the relatively slow propagation of the decalcification front [1], concrete leaching becomes an important matter for the long-term durability of underground structures for nuclear waste disposal, whose life time service should be about tens or hundreds of thousands of years. This issue has motivated many approaches proposed in literature to model the decalcification of cement-based materials (e.g. [1,2,5,6]).

The scope of the present article is two-fold. Its first objective consists in developing an original tool to model and simulate the leaching of cementitious materials and the second one is to predict the impact of this chemical alteration on their elastic properties. Numerous investigations dedicated to the influence of calcium leaching on the residual mechanical behaviour of cement-based materials (e.g. [3,4,7–10]) have concluded on the significant reduction of their elastic moduli and of their residual strength. A method is consequently proposed in this study to estimate this loss of stiffness, which is an important data for assessing the long-term mechanical behaviour of concrete infrastructures. A sequel of the present paper [11] will be devoted to the diminution of the material's residual strength and to the couplings between decalcification and damage.

Although many works already deal with the modelling of the decalcification of cement-based materials, most of them assume that only calcium ions govern the chemical equilibrium (e.g. [6,8,10,12–15]) and/or that the material diffusivity only depends on its porosity

* Corresponding author. Lafarge Centre de Recherche, L'isle D'abeau 95, rue du Montmurier BP 70, 38291 Saint Quentin Fallavier Cedex France. Tel.: +33 4 74 82 16 30.
E-mail address: eric.stora@lafarge.com (E. Stora).

0008-8846/$ – see front matter © 2009 Elsevier Ltd. All rights reserved.
doi:10.1016/j.cemconres.2009.05.010

Nomenclature

c_r	volume fractions of phase r
c_r^{inn}	relative volume fraction of phase r in the inner coating of a doubly coated sphere
c_r^{out}	relative volume fraction of phase r in the outer coating of a doubly coated sphere
C_a	calcium concentration in the pore solution (in mol/L of solution)
C_j	concentration of aqueous species j in the pore solution (in mol/L of solution)
D_r	diffusion coefficient of an isotropic phase r ($m^2\ s^{-1}$)
D_{inn}^*	diffusion coefficient of the inner layer
D_{out}^*	diffusion coefficient of the outer layer
$\mathbf{D}_{HCP}^*$	effective diffusion tensor of the hardened cement paste ($m^2\ s^{-1}$)
e_j	aqueous specie
e_{ja}^{z+}	aggressive ionic specie
e_m	mineral specie
E_r	Young modulus of phase r
K_m	equilibrium balance of the dissolution of e_m
K_{HCP}^*	effective Young modulus of the hardened cement paste
K_r	bulk modulus of phase r
K_j^M	bulk modulus of the matrix phase of layer j
K_{HCP}^*	effective bulk modulus of HCP
G_r	shear modulus of phase r
G_j^M	shear modulus of the matrix phase of layer j
G_{HCP}^*	effective shear moduli of HCP
Mi	number of mineral phases
N	number of aqueous species in the interstitial solution
p_m	concentration of e_m (in mol/L of solution)
S_a	calcium concentration in the solid phase (mol L^{-1})
V_m	molar volume of e_m (in L/mol of solution)
$\mathbf{1}$	second-order identity tensor
J_i	macroscopic flux vector of aqueous species i
$\overline{\mathrm{J}_i}$	microscopic flux vector of aqueous species i
$\mathbb{C}_r$	stiffness tensor of particulate phase r
$\mathbb{C}_M$	matrix stiffness tensor of the matrix phase
$\mathbb{C}_{HCP}^*$	macroscopic stiffness tensor of the hardened cement paste
$\mathbb{J}$	deviatoric operator
$\mathbb{K}$	hydrostatic operator
α_j^M	hydrostatic part of the Eshelby tensor
γ_j^M	deviatoric part of the Eshelby tensor
ν_r	Poisson ratio of phase r
β_i^j	polarizibility of phase i with respect to phase j
χ	stoechiometric coefficients
γ_i	activity coefficient

(e.g. [1,16–18]). To avoid adopting these simplifying hypotheses, an approach is proposed to model leaching processes by combining the benefits of homogenization techniques and the computation power of a numerical platform. Upscaling methods (e.g. [19]) present the salient feature of linking microscopic phenomena, such as phase dissolution or precipitation, to the material's macroscopic behaviour. Furthermore, these methods can be applied to any cement-based material, provided its initial composition and the physical properties of its elementary phases are known. In a previous paper [20], a multi-scale homogenization model was developed and validated to estimate the diffusion coefficients of hardened cement pastes (HCP). In the present work, this homogenization approach is also applied to compute the elastic properties of HCP and extended to the cases of mortars. This analytical model is then incorporated into the ALLIANCES platform [21] developed by the French Atomic Energy Commission (CEA), French National Agency for Nuclear Waste Management (ANDRA) and Electricité de France (EDF). This numerical integration platform is capable of simulating problems that couple chemistry, transport and mechanics [21] by gathering within the same simulation environment a code solving the chemical equilibrium and a finite volume or element software dealing with transport and mechanical problems. The combination of this multi-scale model and the ALLIANCES platform thus permits to develop an advanced tool for predicting how the mineral composition of a concrete material and its elastic and diffusive properties are affected during a degradation process.

The present paper comprises two main parts. The first section is dedicated to the construction of a multi-scale homogenization model for predicting the elastic and diffusive properties of cement-based materials. The second one is specifically devoted to the modelling and simulations of chemical deteriorations of concrete materials. After a brief presentation of how to model the latter degradations with the ALLIANCES platform, simulations of pure water leaching of cement-based materials are thus proposed and validated by confronting with available experimental data.

2. Construction of a multi-scale homogenization model for estimating the elastic and diffusive properties of cement-based materials

The characteristic sizes of the phases composing HCP and mortars range from nanometer to millimeter scales. The scope of the present section is thus to present a realistic multi-scale homogenization approach for these materials integrating some significant information about the different sizes of their particulate phases.

2.1. A multi-scale description of HCP and mortars microstructure

Diverse homogenization models have been developed for estimating the linear elastic effective properties of cement pastes and mortars or predicting their macroscopic diffusivities (e.g. [22,23]). However, these models are generally specifically designed for determining either the effective elastic moduli or macroscopic diffusivities of the material. It is consequently of high interest to develop a unified homogenization approach that is capable of predicting both the mechanical and transport properties of concrete materials on the basis of a realistic microgeometry.

The proposed multi-scale description of HCP has been presented in a previous paper [20] devoted to the estimation of the diffusivities of HCP. In the present article, this model recalled below is applied to estimate the effective elastic properties of HCP and is subsequently extended to the case of mortars. Two microstructural levels respecting the scales separation condition are presently distinguished. The first representative volume element (RVE) encloses hydrated cement grains whose sizes typically range from a few μm to about 100 μm. The size of the first RVE is then about 300 μm, since it should be at least three times bigger than the size of the biggest heterogeneity [24]. The second RVE with an approximate length of 10 μm (Fig. 1) contains inclusions of CH, AF and large capillary pores, whose sizes are considered to range roughly from 0.2 μm to a few μm [25]. The assumption that CH, AF and these pores are smaller than the dimensions of hydrated cement particles is supported by experimental observations [25–28]. These two scales are respectively denoted as I and II.

The level I corresponding to the biggest scale of HCP is described first. This level depicted in Fig. 1 represents the hydrated cement grains. During the hydration of cement particles, two layers presently defined as inner and outer layers form successively from cement grains surface. The inner layer is less porous than the outer one [29], since the first one results from higher confinement conditions and from poorer

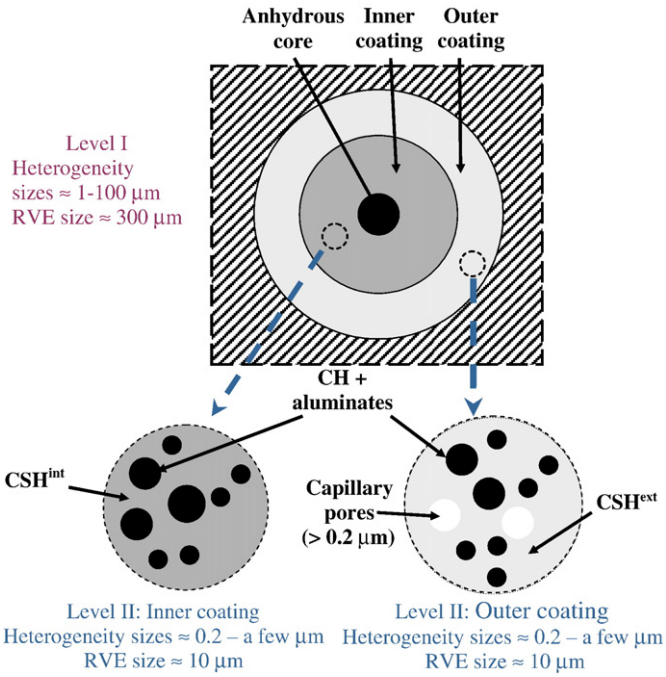

Fig. 1. Schematic of levels I and II of the multi-scale representation used for the estimation of the effective elastic and diffusive properties of HCP.

water accessibility during hydration process. Generally, an anhydrous part of the cement particles remains after hydration has stopped and constitutes a rigid core surrounded by these two heterogeneous layers. The resulting HCP microstructure is consequently modelled as a doubly coated spheres pattern (Fig. 1). The intermediary layer surrounding the core is heterogeneous, with a high-density type of CSH called CSH^{int} embedding inclusions of portlandite and aluminous phases. The external layer consists in a heterogeneous mixture composed of a low-density type of CSH, denoted as CSH^{ext}, CH and AF inclusions and of large capillary pores. The doubly coated sphere representing the hydrated cement grains is immerged in the yet unknown effective medium so as to account for the interactions between these particles. The radii of the core and coatings and the volume fractions of the different phases inside the layers are chosen so that the coated-sphere has the same composition as the original cement paste. The generalized self-consistent scheme (GSCS) [30,31] that is suited for estimating the elastic properties of composite with layered inclusions is thus employed to compute such a model of microstructure. The present description is based on the assumption that the cement grains are supposedly initially spherical hydrate forming doubly coated spheres that fill the HCP microstructure. The spherical particle approximation was shown to be quite reasonable for modelling unhydrated clinker (UC) in [32], since the remaining volume fraction of UC in HCP is usually low.

The level II also depicted in Fig. 1 corresponds to the scale of the heterogeneities of the two layers. In the inner layer, the CSH^{int} behave as a matrix phase embedding inclusions of CH and AF. The external layer has a similar morphology, where CH, AF and large capillary pores play the role of inclusions enclosed in the CSH^{ext}. During hydration, the outer coatings of the hydrated cement grains expand so that they get in contact with each other and we can assume that these pores get entrapped in the outer coatings. The two layers can be represented as a matrix-inclusion type microgeometry, such as the one depicted in Fig. 1, and can be estimated by means of the interaction direct derivation (IDD) estimate [33] that is versatile, simple of use and appropriate for matrix-inclusion morphologies [32].

Mortars consist of a mixture of cement pastes and of sand particles, whose size ranges from 0.1 mm to 5 mm, in order to improve the packing of these grains. Many studies have evidenced that an interfacial transition zone (ITZ), whose thickness ranges from 15 to 40 μm [34], forms between the aggregate particles and the cement. As in the case of HCP, a doubly coated sphere description is adopted (Fig. 2), where a multi-layered sphere is nested inside an infinitely large region filled by the yet unknown effective medium. The core, the intermediary layer and the outer one of the doubly coated sphere are respectively occupied by sand particles, ITZ and the bulk cement paste. The GSCS, whose widespread use is to predict the elastic and diffusive properties of mortars (e.g. [27,34,35]), is employed to compute the effective properties of the mortar as represented in Fig. 2. Experimental data are difficult to gain on the ITZ elastic properties, since they do not really appear as a homogeneous interface but rather as a graded one [36]. To circumvent this difficulty, many authors have estimated these characteristics of the ITZ from experimental values of mortars by inverse analysis (e.g. [34,35]). Unfortunately, very different values have been identified for the Young modulus of the ITZ from one author to another, as pointed out in [37]. That is why, instead of using an inverse method, it is proposed to compute the ITZ elastic moduli with upscaling techniques. For this purpose, the distribution of the cement phases between the ITZ and bulk paste is estimated following the subsequent reasoning. The compositions of the mortar and of its bulk cement matrix that is assumed to be identical to the plain HCP are first computed by means of the Tennis and Jennings hydration model (see Table 1). The hydration degree is adjusted so as to retrieve the water porosities measured experimentally for the mortar and plain HCP. The volume fractions of the phases engulfed in ITZ are then gained as the difference between the total ones present in the mortar and the volume fractions of the phases comprised in the cement matrix. The different steps of the homogenization process are given in the next subsection.

2.2. Multi-step homogenization process for estimating the elastic and diffusive properties of HCP and mortars

This subsection gathers the main formulae necessary to compute the multi-scale homogenization model. For more information about these equations the reader should refer to [38]. Cement pastes (and mortars) are assumed to be macroscopically isotropic so that the effective diffusion tensor $\mathbf{D}^*_{HCP}$ and stiffness tensor $\mathbb{C}^*_{HCP}$ of HCP are respectively simplified into $\mathbf{D}^*_{HCP}\mathbf{1}$, where $\mathbf{1}$ is the second-order identity tensor and D^*_{HCP} is the scalar diffusion coefficient, and $\mathbb{C}^*_{HCP} = 3K^*_{HCP}\mathbb{J} + 2G^*_{HCP}\mathbb{K}$, where K^*_{HCP} and G^*_{HCP} are the effective

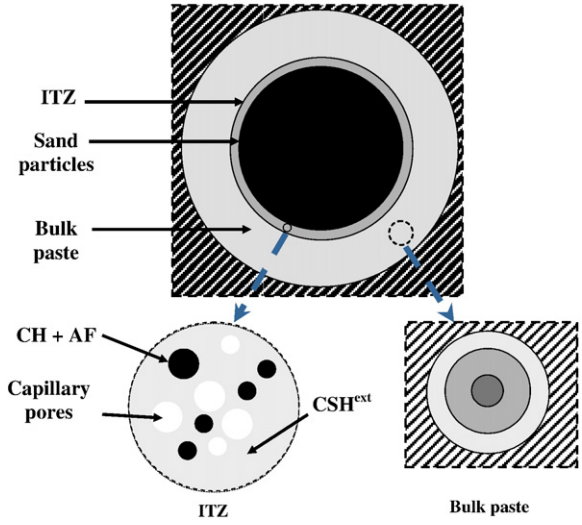

Fig. 2. Schematic of the multi-scale representation used for the estimation of the effective elastic and diffusive properties of mortars.

Table 1
Initial composition in terms of total volume fractions of the CEM I pastes and of the mortars used for the simulations.

Phases	CEM I 52.5 HTS paste (w/c = 0.45) [4]	OPC type I paste (w/c = 0.50) [26]	Mortar (w/c = 0.50) [13]	CEM I 42.5 paste (w/c = 0.40) [7]	Mortar (w/c = 0.40) [7]
Estimated hydration rate	0.87	0.82	0.5	0.8	0.6
CH	0.151	0.113	0.026	0.119	0.045
AFt	0.00	0.086	0.032	0.063	0.024
AFm	0.073	0.042	0.013	0.141	0.053
Hydrogarnet	0.069	0.003	0.00	0.00	0.00
CSH	0.504	0.487	0.089	0.483	0.186
UC	0.043	0.024	0.102	0.074	0.068
Porosity	0.326	0.397	0.270	0.270	0.180
ITZ	–	–	0.217	–	0.104
Sand	–	–	0.50	–	0.50

bulk and shear moduli of HCP and the tensors $\mathbb{J}$ and $\mathbb{K}$ are hydrostatic and deviatoric operators (e.g. [39]).

All the main phases constituting HCP microstructure, namely CH, AF, CSH^{int}, CSH^{ext}, UC and large capillary pores (LCP), are supposed to be isotropic, their total volume fractions, diffusivities, bulk and shear moduli being designated by c_r, D_r, K_r and G_r, respectively. The input data required for the estimations are the volume fractions of the HCP elementary phases collected in Table 1 and their elastic moduli gathered in Table 2. The volume fractions are computed by means of the Tennis and Jennings model [29], the total porosity being adjusted with the total water porosity measured experimentally. The volume fraction of large capillary porosity is taken from the experimental results of Igarashi et al. [41]. CH, AF and UC are considered as non-diffusive and the diffusivities of CSH^{int} and CSH^{ext} are estimated by means of the Mixed Composite Spheres Assemblage (MCSA) model [20], which takes into account the connectivity of gel porosity.

The first step of the homogenization process consists in computing the elastic properties of the two layers of the hydrated cement particles, schematically illustrated in Fig. 1, by means of the explicit IDD estimate [33]. HCP particulate phases are assumed to be spherically distributed and are modelled as spherical inclusions for simplicity reasons and because of the difficulty to characterize their real shape in HCP microstructure. In this case, the IDD scheme coincides with the Mori-Tanaka, Ponte-Castaneda and Willis and Küster-Töksöz estimates. The spherical particle shape approximation works generally quite well provided the volume fractions of inclusions and the contrasts between the inclusions and the matrix are not too strong [32,39,40]. It was more precisely shown in [32] that for HCP the shape of the inclusion modelling particulate phases, such as portlandite, has only a moderate influence on the micromechanical predictions except for leached pastes with a capillary porosity higher than 30%. The more complicated case of portlandite modelled as oblate spheroidal inclusions is computed in [38] but it only gives slightly better results. Under such hypothesis, the IDD scheme yields the following predictions for the effective bulk and shear moduli of the two layers [33]:

$$K_j^* = K_j^M \frac{1 + \sum_r \frac{c_r}{c_j}\left(\frac{K_r}{K_j^M}\alpha_j^M - 1\right)}{1 + \sum_r \frac{c_r}{c_j}\left(\alpha_j^M - 1\right)} \quad \text{and} \quad G_j^* = G_j^M \frac{1 + \sum_r \frac{c_r}{c_j}\left(\frac{G_r}{G_j^M}\gamma_j^M - 1\right)}{1 + \sum_r \frac{c_r}{c_j}\left(\gamma_j^M - 1\right)} \tag{1}$$

$$\text{with} \quad \alpha_j^M = \frac{3K_j^M}{3K_j^M + 4G_j^M} \quad \text{and} \quad \gamma_j^M = \frac{6\left(K_j^M + 2G_j^M\right)}{5\left(3K_j^M + 4G_j^M\right)}, \tag{2}$$

where $j \in \{inn, out\}$, $r \in \{AFt, AFm, LCP, CH, UC\}$, c_j designates the total volume fraction of the layer j in the doubly coated sphere (Fig. 1), α_j^M and γ_j^M represent the hydrostatic and deviatoric parts of the Eshelby tensor (e.g. [39]). The bulk and shear moduli of the matrix phase of layer j are denoted as K_j^M and G_j^M. The subscripts '*inn*' and '*out*' respectively refer to the inner and outer layers, as depicted in Fig. 1. The effective diffusion coefficients D_{inn}^* and D_{out}^* of the inner and outer layers are also estimated by the IDD effective medium theory:

$$D_j^* = D_j^M \left(\frac{1 + 2\sum_r \frac{c_r}{c_j}\beta_j^r}{1 - \sum_r \frac{c_r}{c_j}\beta_j^r}\right), \text{ with } \beta_j^r = \frac{D_j - D_r}{D_j + 2D_r}. \tag{3}$$

In the inner coating, CSH^{int} act as a matrix so that $D_{inn}^M = D_{CSHint}$, $K_{inn}^M = K_{CSHint}$ and $G_{inn}^M = G_{CSHint}$, whereas in the outer layer this role is played by CSH^{ext} so that $D_{out}^M = D_{CSHext}$, $K_{out}^M = K_{CSHext}$ and $G_{out}^M = G_{CSHext}$ (Fig. 1).

The second step consists in determining the HCP effective properties with the aid of the previous result for the inner and outer layers. For this purpose, the doubly coated sphere model depicted in Fig. 1 is computed by means of the implicit GSCS [30,31]. The effective bulk modulus K_{HCP}^* of HCP resulting from the latter scheme takes the following form:

$$K_{HCP}^* = K_{ext} + \frac{c_{UC} + c_{inn}}{1/(K_C - K_{ext}) + 3c_{ext}/(3K_{ext} + 4G_{ext})},$$

with

$$K_C = K_{inn} + \frac{c_{UC}/(c_{UC} + c_{inn})}{1/(K_{UC} - K_{inn}) + 3c_{inn}/(c_{UC} + c_{inn})/(3K_{inn} + 4G_{inn})}. \tag{4}$$

The rather lengthy expression of the shear modulus G_{HCP}^* obtained with GSCS for HCP represented as a doubly coated sphere model is not presently recalled, since it may be found in many articles or manuscripts (e.g. [31,34]). The effective Young modulus E_{HCP}^* and Poisson ratio ν_{HCP}^* of HCP can then straightforwardly be deduced from these macroscopic bulk and shear moduli by the following relations:

$$E_{HCP}^* = \frac{9K_{HCP}^* G_{HCP}^*}{3K_{HCP}^* + G_{HCP}^*} \quad \text{and} \quad \nu_{HCP}^* = \frac{3K_{HCP}^* - 2G_{HCP}^*}{6K_{HCP}^* + 2G_{HCP}^*}. \tag{5}$$

The computation of the effective diffusivity of HCP by means of the GSCS is much simpler than in elasticity (e.g. [27]) and leads to the ensuing estimation of HCP diffusivity:

$$D_{HCP}^* = 2D_{out}^*\left(\frac{3}{2 + c_{UC} - 2c_{inn}\beta_{inn}^{out}} - 1\right). \tag{6}$$

2.3. Estimations of the macroscopic elastic and diffusive properties of mortars

Two mortars, whose total volume fraction occupied by sand is about 50%, are presently considered [7,8,13]. The volume fractions

Table 2
Elastic properties of the main HCP phases in sound and leached states used for the micromechanical calculations.

Phases	Sound HCP		Leached HCP		References
	E (GPa)	ν	E (GPa)	ν	
CH	42.3	0.324	0	0	[55]
Unhydrated clinker	117.6	0.314	117.6	0.314	[56]
Capillary pores	0	0	0	0	
AFt, C_4AH_{13}, hydrogarnet	22.4	0.25	0	0	Assumed by [58]
AFm	42.3	0.324	0	0	Assumed by [58]
CSH^{ext}	21.7	0.24	3	0.24	[26]

occupied by ITZ are difficult to gain experimentally, because the diverse ITZ layers tend to overlap and the thickness of the ITZ layers is generally observed to be independent from the particle sizes [13,42]. In the present description, the thickness of the ITZ is assumed to be constant and equal to 20 μm [13]. The mid sand aggregate sizes being about 750 μm for the mortar from Le Bellégo [7] and 350 μm for the one from [13], the volume fractions occupied by the ITZ thus obtained are about 10.4% and 21.7%, respectively.

A simple but coherent method is proposed for estimating how the diverse phases are dispersed in ITZ and the bulk cement paste (Fig. 2). As for the plain HCP, the composition of the two mortars is computed by means of the Tennis and Jennings hydration model (see Table 1), the total porosity thus obtained being adjusted with the water porosity measured experimentally. The cement matrix of the two mortars are then supposed to have exactly the same composition as the plain cement pastes, whose compositions are also given in Table 1. The volume fractions of the different phases scattered in ITZ are finally taken in such a way that the total volume fractions of these phases inside the mortar are retrieved. The porosities inside the ITZ obtained with this method are about 70% for the two mortars. These high porosities agree with experimental investigations observing that the ITZ is more porous than the cement paste [36].

The elastic moduli of the mortar can be estimated by the multi-scale upscaling approach represented in Fig. 2 with the help of the volume fractions determined just above. The Young modulus and the Poisson ratio of the sand aggregates are respectively taken equal to 62.5 GPa and 0.21 [13]. The effective properties of ITZ and of the bulk cement paste schematically represented in Fig. 2 as matrix-inclusion microgeometries are evaluated by homogenization. The elastic and diffusive characteristics of ITZ are computed by means of the IDD estimate in Eqs. (1)–(3) and the bulk cement paste ones are estimated by the multi-scale model developed in the preceding subsection. The elastic and diffusive properties of the mortar are then predicted from Eqs. (4) and (5) with the aid of the previous results for ITZ and bulk cement pastes. The elastic moduli of the plain cement pastes and mortars predicted by the present multi-scale homogenization model are then confronted in Table 3 with different experimental results on sound specimens [4,7,13,25] but also on uniformly leached ones. Indeed, Ulm et al. [13,23] measured that the stiffness moduli of a uniformly leached standard paste and mortar decreased to about 3 Gpa and 4.8 Gpa respectively representing decays superior to 80%. To obtain a uniformly degraded material, the samples with a diameter of 11.5 mm were attacked by an ammonium nitrate solution during 5 months. The predictions of the proposed model are in good agreement with the experimental data displayed on Table 3, which validate to a certain extent the present approach.

In [20], the estimations of the HCP diffusivities by the present multi-scale homogenization model have moreover been validated by comparing them with the experimental measurements on sound CEM I pastes with diverse w/c ratios [43]. In the present article, this multi-scale approach is further applied to compute the effective diffusivity of the mortar used by Bourdette [44] and Le Bellégo [7] with the help of the input parameters collected in Table 1. The value thus obtained, 1.8×10^{-12} m^2/s, is close to the experimental diffusivity, i.e. 1.7×10^{-12}m^2/s, measured by Bourdette [44]. The present multi-scale model, whose estimations are in good agreement with the experimental data, is incorporated in the ensuing section in the ALLIANCES platform to simulate leaching processes in cement-based materials and their effects on the material's residual elastic behaviour.

Table 3
Comparison of the micromechanical estimations with experimental data on cement pastes and mortars.

Materials	Young modulus predicted (GPa)		Young modulus measured (GPa)		References
	Sound	Leached	Sound	Leached	
OPC Type I paste w/c = 0.50	23.1	3.0	22.8	3.5	[13]
CEM I HTS w/c = 0.45	23.7	–	23	7.0*	[4]
Mortar w/c = 0.50	27.4	5.3	25.1	4.8	[13]
Mortar w/c = 0.40	38.2	4.9	38.5	–	[7]

*Not a uniformly leached specimen.

3. Simulations of the chemo–mechanical behaviour of leached cement-based materials

3.1. Presentation of ALLIANCES

The scope of this section is to detail the main steps for modelling chemical degradations of cement-based materials with the ALLIANCES platform that is briefly presented below. For more details concerning the latter platform, the reader should refer to [21]. The ALLIANCES platform allows for combining and connecting together diverse numerical codes dealing with different physical problems. This platform is developed in collaboration between CEA, ANDRA and EDF for the simulation of nuclear waste disposal. This tool programmed in Python is employed in the present paper and its companion one [20] to couple chemistry, with the code CHESS [45], transport and mechanics, with the finite volumes and elements software CAST3M (CEA), so as to perform numerical simulations of the multi-physical degradation of cement-based materials. In the present context of long-term deterioration of concrete underground structures in the nominal phase of waste storage, the following simplifying assumptions are made:

- the material is in saturated and isothermal conditions;
- electro-diffusive phenomena are neglected, ionic transfers being only due to molecular diffusion;
- the same diffusion coefficient is affected to all aqueous species;
- chemical reactions are instantaneous compared to the diffusion process.

3.2. Coupled chemical-transport problem solved by ALLIANCES

A concrete material is considered to be in contact with an aqueous solution. The existence of concentration gradients of ions between the interstitial solution and the aqueous one provokes ionic migration inside the interstitial solution, governed by the material's transport properties. This movement of ions disturbs the chemical equilibrium state between the solid skeleton and the pore solution of the material and causes dissolution–precipitation reactions in the material. It is then necessary to perform coupled chemo-transport simulations to reproduce such degradation.

Different types of chemical-transport simulations have been performed on concrete materials (e.g. [1,6,16–18,46,47]). Simplified approaches have first been proposed (e.g. [1,6]), where only calcium ions are supposed to govern the main chemical reactions. More advanced simulations capable of treating multi-species reactive transport problems are also available (e.g. [46,47]), where the current chemical equilibrium state is obtained by means of a chemical equilibrium code. This is important in the case of decalcification for modelling for instance the migration of alkalis or simulating accelerated leaching by ammonium nitrate (NH_4NO_3) because of the penetration of NO_3^-. Indeed, aggressive solutions such as NH_4NO_3 are frequently used by experimentalists to enhance the degradation process [3]. In particular, a very concentrated solution containing 6 mol/L (6 M) of NH_4NO_3 is generally employed for the coupled chemo–mechanical degradation experiments (e.g. [7]). The present paper limits itself for conciseness to the degradation of small cement samples by pure water but accelerated leaching tests by a 6 M NH_4NO_3 solution will be simulated in a subsequent contribution [11] so as to reproduce available chemo–mechanical degradation experiments [7].

The ALLIANCES platform solves multi-species reactive transport problems by coupling the chemical equilibrium code (CHESS) with transport (finite volume CAST3 M) in the following manner:

$$\begin{cases} \dfrac{\partial (c_P C_i)}{\partial t} = \mathrm{Tran}(c_P, c_m, C_i), \\ (C_i, p_m) = \mathrm{Ch}_{0i}(C_i), \\ c_P = \left(1 + \sum_{m=1}^{M} V_m p_m\right)^{-1}, \forall i \in \{1, \ldots, N\}, \forall m \in \{1, \ldots, Mi\}, \end{cases} \quad (7)$$

where c_m, c_P respectively denote the volume fractions of the mineral phase m and the porosity, C_i, p_m, V_m respectively designate the concentrations of the aqueous species, of the mineral m and the molar volume (L/mol) of the mineral m. The medium initially comprises Mi mineral phases supposedly homogeneous and contains N aqueous species, most of them being ions. The operators Tran and Ch, respectively computed by CAST3M and CHESS, are such as:

$$\mathrm{Tran}(c_P, c_m, C_i) = div\left(\mathbf{D}^*(c_P, c_m).\overrightarrow{\mathbf{grad}(C_i)}\right) \quad (8)$$

$$\mathrm{Ch}_{0i}(C_i) = \begin{cases} \text{precipitation} & K_m^p = \prod_{i=1}^{N} [e_m]\left[e_i^{z+}\right]^{-\nu_{im}}, \\ \text{dissolution} & K_m^d = \prod_{i=1}^{N} \left(\left[e_{ia}^{z+}\right][e_m]\right)^{-1}\left[e_i^{z+}\right]^{\nu_{im}}, \end{cases}$$

where K_m^d and K_m^p are the equilibrium constants of the dissolution or precipitation reactions, ν_{im} designates the stoechiometric coefficients, e_m denotes a mineral specie, e_{ia}^{z+} an ionic specie consumed in the dissolution reaction and e_i^{z+} an aqueous specie that forms in the interstitial solution, z being an integer. The square brackets surrounding a given specie designate its activity that is computed by means of the modified Davies method.

The multi-species reactive transport problem described in Eqs. (7) and (8) is solved by means of a sequential iterative algorithm [48], each chemical-transport loop being evaluated in the following manner. The first step consists in computing with CAST3M the transport of aqueous species by means of the finite volume method. The medium is thus represented by a number w of subvolumes V_l each comprising Mi mineral phases and N aqueous species. A fixed point algorithm implicit in time is used to solve the transport equations [49]. For simplicity, the cinematic dispersion is neglected. The material's effective diffusivity in each subvolume is estimated from its current composition by implementing the multi-scale homogenization model into ALLIANCES.

By communicating with a chemical equilibrium code (CHESS), ALLIANCES in a second step updates the mineral composition and the porosity of the cement at each time step and re-evaluates by means of the homogenization model the evolution of the diffusivity inside the material from its current composition. The scheme employed to solve this chemical part is explicit. The precision concerning the chemical resolution is fixed by the user and is defined at a given time step $t+1$ from the total concentration of the constituting species as follows:

$$\frac{\|F^{t+1,l+1} - F^{t+1,l}\|}{\|F^{t+1,l+1}\|} < Pr, \quad \text{with} \quad F^{t+1,l} = \sum_j \sum_{m=1}^{Mi} \chi_{jm} p_m (l \in \{1, \ldots, I_{max}\}), \quad (9)$$

where Pr designates the precision, l is the iteration index and $I_{\max}$ is the maximal number of iterations desired. ALLIANCES then adapts the time steps so that convergence is obtained within this number of steps. It is often necessary to impose a precision less than 10^{-6} resulting in small time steps, practically a few hundreds of seconds, to ensure convergence of the computations. In the ensuing subsection, simulations of pure water leaching of HCP are carried out with the help of the numerical methods presented just above.

3.3. Simulations of pure water leaching tests of HCP

The following system (Fig. 3) is adopted for modelling the pure water leaching process of HCP. A hydrated cement paste sample, simply modelled as a rectangle with 3 mm of length and 1 mm of height, is in contact on its left extremity with pure water (pH = 7), while a zero flux condition is imposed on the other one. The mesh used is composed of 30 rectangular subvolumes. The computations of the chemistry-transport loop provide the mineral composition at each center of the subvolumes. For simplicity, alkalis (Na^+, K^+) are not taken into account in the interstitial solution, since they rapidly disappear during the leaching process according to [1,46]. Consequently, the pH of the interstitial solution is fixed by the equilibrium with portlandite and is initially about 12.5. The temperature considered constant is 25 °C.

The first chemical input data necessary for simulating the pure water degradation of a concrete material are the concentrations of the initial mineral species, p_m, which can be computed by dividing the phase volume fractions collected in Table 1 with their molar volumes given in [29]. In order to obtain reasonable computations times, non altered HCP is assumed to be composed only of five main phases: [UC, CH, AFm, $C_{1.65}SH$, and AFt or hydrogarnet]. During the leaching simulations, the chemical code CHESS searches for the new mineral phases that may potentially precipitate using its huge database. To further decrease the time computation, the database is reduced to the following system for altered HCP: [CH, AFt, AFm, $C_{1.65}SH$, $C_{1.25}SH$, $C_{0.90}SH$, SiO_2(am), diaspore, gypsum, and hydrogarnet], where SiO_2 (am) refers to the amorphous silicon gel. The chemical formulae and the equilibrium constants of these mineral phases are given in Table 4.

In contrast to portlandite that can totally dissolve during the degradation of a cement paste, the decalcification of CSH rather implies a progressive decrease of their C/S ratio. As a consequence, their diffusive and elastic properties are gradually diminished. To model this degradation in a simplified way, three types of CSH with diverse C/S ratios (C/S = 1.65, 1.25, 0.90) corresponding to more or less decalcified states, are introduced in CHESS. Silicon gel SiO_2(am) is furthermore introduced in the chemical system to represent the most

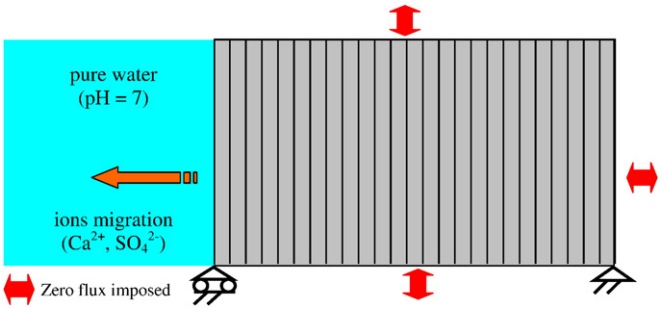

Fig. 3. Schematic of the one-dimensional system employed for the simulations of pure water leaching of HCP.

Table 4
Chemical formulae and equilibrium constants of the mineral phases in the reduced database.

Mineral phases	Chemical formula	Equilibrium constant	References
CH	$Ca(OH)_2$	$10^{-22.90}$	[58]
AFt	6 $CaO–Al_2O_3–3\ SO_3–24\ H_2O$	$10^{-57.00}$	[58]
AFm	4 $CaO–Al_2O_3–SO_3–12\ H_2O$	$10^{-70.25}$	[58]
Hydrogarnet	3 $CaO–Al_2O_3–6\ H_2O$	$10^{-78.80}$	[58]
$C_{1.65}SH$	1.65 $CaO–SiO_2$(aq)–1.65 H_2O	$10^{-29.36}$	[58]
$C_{1.25}SH$	1.25 $CaO–SiO_2$(aq)–1.25 H_2O	$10^{-20.25}$	[58]
$C_{0.90}SH$	0.90 $CaO–SiO_2$(aq)–0.90 H_2O	$10^{-13.01}$	[58]
SiO_2(am)	SiO_2(aq)	$10^{+2.16}$	[45]
Diaspore	AlO_2H	$10^{-7.13}$	[45]
Gypsum	$Ca(SO_4)–2\ H_2O$	$10^{-4.48}$	[45]

decalcified state of CSH. The CSH^{int} and CSH^{ext} are not distinguished in the chemical computations, since their relative proportions inside the paste are not affected by leaching [23]. They are however differentiated by means of the formula of Tennis and Jennings [29] in the multi-scale homogenization model presented in Section 2, because they have different elastic and diffusive properties. Constantinides and Ulm [23] have measured the Young moduli of CSH^{int} and CSH^{ext} both for sound and uniformly leached states, their C/S ratio decreasing to 0.8 [13]. It is supposed that the effective diffusivities and Young moduli of the two heterogeneous CSH evolve as a function of their C/S ratios comprised between 0.8 and 1.65 in the following manner:

$$\begin{cases} \text{if } C/S > 0.8, & E_{CSHint\ or\ ext} = \left(1 - \dfrac{C/S - 0.8}{1.65 - 0.8}\right) E^{UL}_{CSHint\ or\ ext} + \dfrac{C/S - 0.8}{1.65 - 0.8} E^{S}_{CSHint\ or\ ext}; \\ \text{if } C/S \le 0.8, & E_{CSHint\ or\ ext} = E^{UL}_{CSHint\ or\ ext}, \end{cases}$$

$$\begin{cases} \text{if } C/S > 0.8, & D_{CSHint\ or\ ext} = \left(1 - \dfrac{C/S - 0.8}{1.65 - 0.8}\right) D^{UL}_{CSHint\ or\ ext} + \dfrac{C/S - 0.8}{1.65 - 0.8} D^{S}_{CSHint\ or\ ext}; \\ \text{if } C/S \le 0.8, & D_{CSHint\ or\ ext} = D^{UL}_{CSHint\ or\ ext}, \end{cases} \quad (10)$$

where the superscripts *S* and *UL* mean sound and uniformly leached, respectively. The values of the Young moduli $E^{S}_{CSHint\ or\ ext}$ and $E^{UL}_{CSHint\ or\ ext}$ are taken from Constantinides and Ulm [23] and the diffusivities $D^{S}_{CSHint\ or\ ext}$ and $D^{UL}_{CSHint\ or\ ext}$ are estimated by means of the MCSA model developed in [50]. For computing $D^{UL}_{CSHint\ or\ ext}$, it is assumed that a total volume fraction 0.065 of additional gel porosity arises in the CSH in their most leached state [38]. The Poisson ratio is considered to remain constant during the leaching process [23]. The anhydrous residuals are furthermore assumed to be unreactive, since they only represent a few percent in terms of volume fractions and modelling their hydration would require very long computation times. With this system, the following chemical species mainly appear in the interstitial solution: [Ca^{2+}, SO_4^{2-}, Al^{3+}, and SiO_2(aq)].

In order to perform a rigorous validation of the simulations and investigate the influence of the composition of the cement pastes on their chemical degradations, two CEM I pastes, that are well characterized [1,51,52] and whose mechanical behaviour has also been studied [3,4,7,46] are employed: a CEM I 42.5 of Origny with w/c = 0.40 [7,53] and a CEM I 52.5 HTS with w/c = 0.45 from Lafarge [4,46]. The comparison between the two cement pastes provides furthermore some insights about the effects of the hydration rate and of the w/c ratio on the chemical degradation. The CEM I 52.5 HTS and CEM I 42.5 pastes have quite different initial compositions. The latter given in Table 1 are obtained with the aid of the Tennis and Jennings model [29] for the CEM I 52.5 HTS paste and of the simplified model from [1] for the CEM I 42.5 one. The hydration rates are estimated in the calculations of the phase volume fractions so as to retrieve a total porosity equal to the water porosity measured experimentally [4,7,54].

Fig. 4 presents the mineral profiles in the CEM I HTS and CEM I 42.5 pastes leached with pure water during 50 days. The successive complete dissolution of CH, hydrogarnet, AFm and AFt, may be observed in this figure. These sequences of dissolution are in good accordance with the experimental observations (e.g. [1,57]). It is moreover noteworthy that AFt reprecipitates in the zone where AFm has dissolved, as is habitually viewed experimentally. Lower C/S ratio CSH, $C_{1.25}SH$ and $C_{0.90}SH$, successively precipitate near the interface with pure water, which allows for an accounting in a simplified manner of the progressive decalcification of CSH.

The dissolution front of portlandite in Fig. 4 propagates faster in the CEM I HTS paste than in the CEM I 42.5. Fig. 5 confirms that the degradation propagates faster in the CEM I HTS paste. The decrease of the pH and of the concentration of calcium in solid and liquid phases is much more significant than inside the CEM I 42.5 paste due to the faster decalcification of CSH and CH. These profiles strongly depend on the presence of CH. Indeed, the calcium concentration in the solid phase decreases as soon as CH starts to dissolve. Furthermore, its presence controls the pH and the calcium concentration in the solution and both decrease whenever CH is totally dissolved. The dissolution front propagations obtained numerically for the two pastes are confronted in Table 5 with experimental results issued from pure water leaching tests [1,4]. They appear to underestimate by about 20% the degradation front propagation measured experimentally but the calcium fluxes are in better agreement with the experimental values.

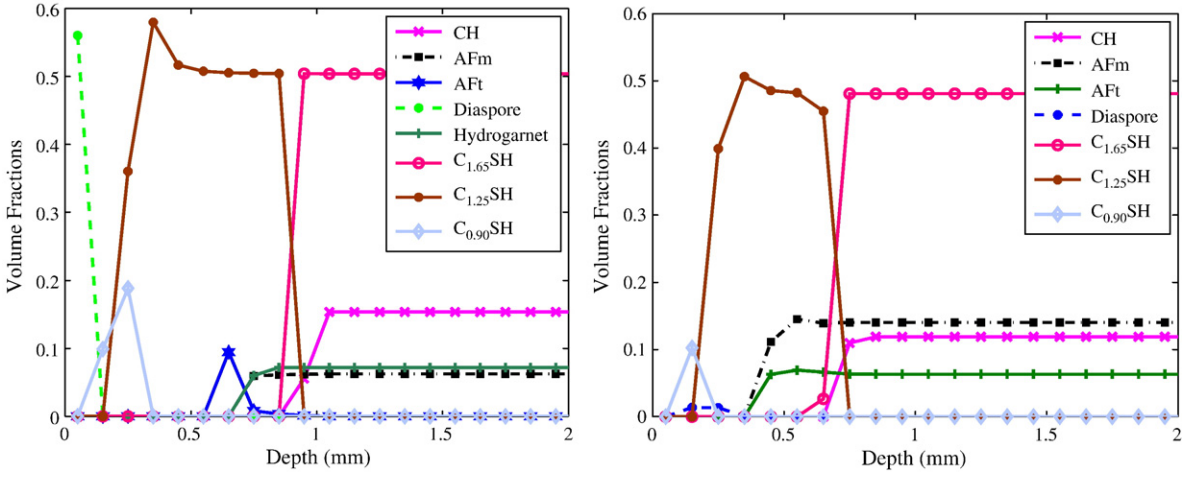

Fig. 4. Mineral compositions in terms of volume fractions inside a sample of CEM I 52.5 HTS paste with w/c = 0.45 and of CEM I 42.5 one with w/c = 0.40 subjected to a 50 days attack by pure water simulated with ALLIANCES, respectively.

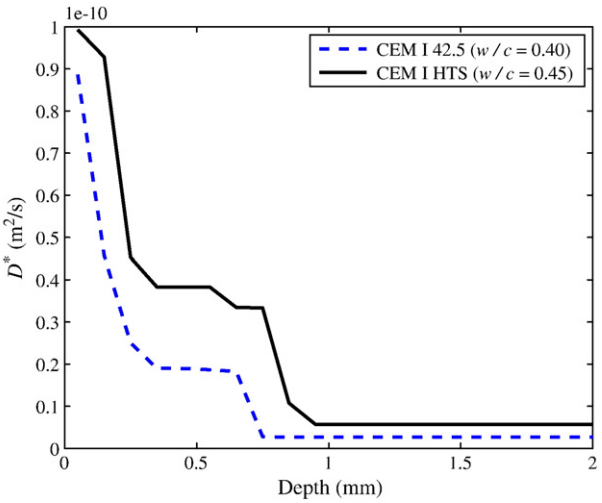

Fig. 5. Evolutions of the diffusivities predicted with the multi-scale homogenization model inside samples of CEM I 42.5 (w/c = 0.40) and of CEM I HTS (w/c = 0.45) pastes after a 50 days attack by pure water simulated with ALLIANCES.

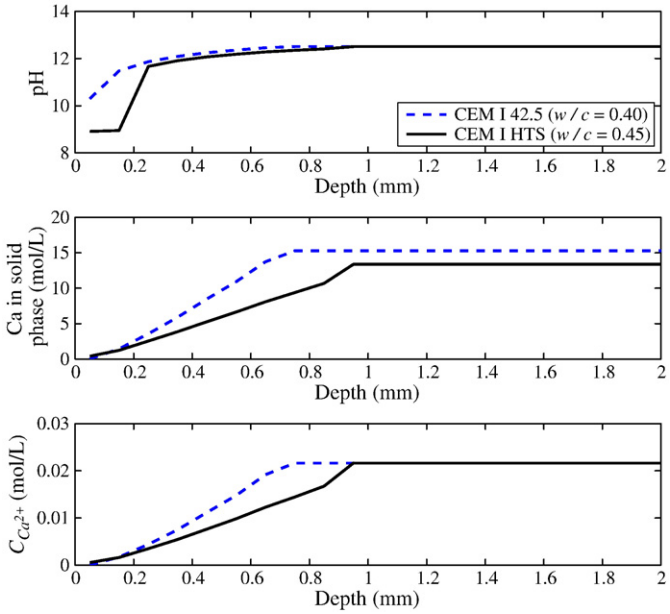

Fig. 6. Evolutions of the pH of the interstitial solution (up) and of the concentrations of calcium ions in solid phase (middle) and in solution (down) inside CEM I 52.5 HTS (w/c = 0.45) and CEM I 42.5 (w/c = 0.40) pastes subjected to a 50 days attack by pure water simulated with ALLIANCES.

A plausible explanation for this underestimation of the leaching front is the fact that the diffusivity of the leached zone is underestimated.

As a complement, Fig. 6 thus shows that the diffusion coefficients inside the two CEM I pastes increase by more than one order of magnitude in the chemically altered zone due to the additional porosity created by the dissolution of certain mineral phases. This augmentation seems very high to us at first sight but, unfortunately, we lack the experimental data to validate the diffusion coefficients for the leached zone. The diffusivity inside the leached pastes appears to be strongly affected in a first step by the dissolution of the CH and in a second one by the progressive decalcification of the CSH. It is furthermore seen in Fig. 5 that the diffusivity inside the CEM I 52.5 HTS is always higher than inside the CEM I 42.5 one, since the CEM I 52.5 HTS is initially more porous and has a higher diffusivity (see Tables 2 and 3). This explains why the dissolution front of portlandite propagates faster in the CEM I HTS paste than in the CEM I 42.5. An additional possible reason why the CEM I 42.5 paste resists better to leaching than the other one is that it contains less portlandite and more aluminates showing a better resistance to pure water.

3.4. Stiffness reduction of cement-based materials after leaching

The multi-scale homogenization approach developed to estimate the evolutions of the diffusivity of cement-based materials is also applied to predict their elastic properties in both sound and leached states. The Young moduli of each subvolume of the simulated cement-based material can be estimated by implementing this model into ALLIANCES. The volume fractions of each mineral phase necessary for applying the homogenization model are provided by the previous simulations of the chemical deterioration. The volume fractions given in Fig. 4 and the measurements by nanoindentation of the elastic properties of each mineral phase (see Table 2) then serve as input parameters for the estimations plotted in Fig. 7 for the Young modulus of the CEM I 42.5 inside the degraded sample. The latter modulus is significantly reduced in the altered zone because of the dissolution of rigid phases, such as CH and AF. It may be seen in Fig. 7 that the decrease occurs in two steps: the first one is attributed to the dissolution of CH and the second one is caused by the decalcification of the CSH. This sharp diminution due to leaching is in good agreement with the experimental works of [3,4,23] that evidence a significant effect of leaching on the macroscopic Young modulus of cement pastes. Constantinides and Ulm [23] further measured that the stiffness modulus of a uniformly leached paste decreased to about 3 GPa. The homogenized Young modulus of the most decalcified subvolume on the left-hand side of Fig. 7 is of the same order. The tool

Table 5
Comparison of the decalcification front propagations obtained in the simulations performed with ALLIANCES of pure water leaching with experimental values.

Decalcification front propagation	Origny CEM I 42.5 paste w/c = 0.40	Lafarge CEM I 52.5 HTS paste w/c = 0.45
Experimental decalcification front propagation	0.15 mm $d^{-0.5}$ [1]	0.19 mm $d^{-0.5}$ [4]
Simulated decalcification front propagation (after 50 days of pure water leaching)	0.12 mm $d^{-0.5}$	0.15 mm $d^{-0.5}$
Calcium flux measured experimentally	1.4 mol m^{-2} $d^{-0.5}$ [1] 1.1 mol m^{-2} $d^{-0.5}$ [44]	1.75 mol m^{-2} $d^{-0.5}$ [4]
Simulated calcium flux (after 50 days of pure water leaching)	1.0 mol m^{-2} $d^{-0.5}$	1.7 mol m^{-2} $d^{-0.5}$

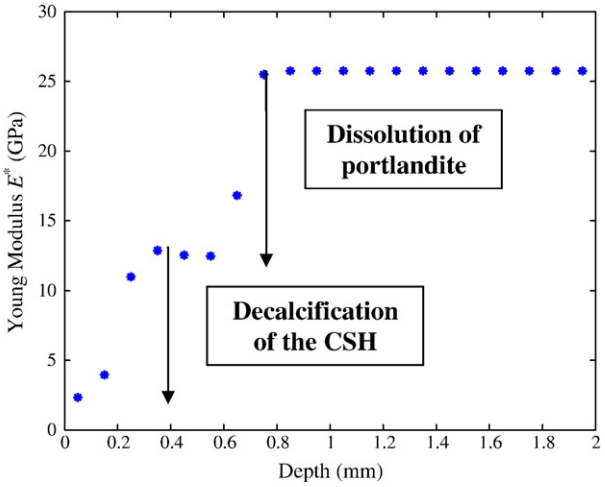

Fig. 7. Evolution of the Young modulus inside a sample of CEM I 42.5 paste with w/c = 0.40 subjected to a 50 days pure water attack.

presently developed is thus capable of estimating the residual linear elastic properties of leached concrete materials. Its extension to predict the material's non-linear mechanical response and the possible interactions between damage and leaching is reported in [11,38].

4. Conclusions

The present work is devoted to the development of a tool incorporated in the ALLIANCES numerical platform that allows for predicting the evolutions of the mineral composition of leached cementitious materials and of their elastic properties. The originality of this approach lies in the utilization of a multi-scale homogenization approach to estimate the evolutions of the diffusivity and the elastic behaviour of cement-based materials. The upscaling techniques constitute a precious instrument to model the effects of microstructure on the material's physical properties. For the leaching processes presently studied, they have enabled to correlate in a relatively simple manner the dissolution of hydrated phases, such as CH, represented as rigid and impermeable inclusions to the decrease of the Young modulus and augmentation of the material's diffusivity. The reader should however keep in mind that these efficient homogenization methods based on simple microgeometries cannot capture all the complexities of the random microstructure of cement-based materials and provide estimations bearing some uncertainties. But the joint progress in microstructure characterization [59,60] and upscaling approaches applied to cement-based materials [61–63] could lead to more precise predictions in the oncoming years.

Pure water leaching tests of cement pastes have been simulated and their loss of stiffness has then been investigated. The numerical results confronted with experimental tests [1,4,7] are encouraging and give the following valuable insights. First, the diffusivity inside the leached parts of these materials increases stepwise according to our model by more than one order of magnitude, while the Young modulus in these decalcified zones can decrease by more than 80%. More precisely, these properties are first strongly affected by the dissolution of portlandite and in a second time by the progressive decalcification of CSH. These results are of course not new but appear to be more precise than those obtained with simplified approaches (e.g. [6]). The applications of the proposed numerical tool can furthermore be extended to real concrete underground structures and to diverse types of chemical attacks, such as sulphatic attacks generating internal pressures and possibly microcracks.

The present simulations confronted with available experimental data have been performed for relatively short periods. Indeed, the effects of leaching by water at the scale of a real concrete structure are only observable for very long times, since it roughly takes 300 years to leach 4 cm of a concrete structure by extrapolating results from leaching experiments [1,7]. In order to better assess the long-term behaviour of cementitious materials, accelerated leaching of mortar beams equivalent to a few decades of decalcification by pure water and the resistance of these degraded beams to flexion tests have also been simulated and is presented in [11,38].

Acknowledgements

Financial support from DSNI/Réacteurs is acknowledged.

References

[1] F. Adenot, Durabilité du Béton: Caractérisation et Modélisation des Processus Physiques et Chimiques de Dégradation du Ciment, PhD Thesis, Université d'Orléans, France, 1992 (in French).
[2] F. Adenot, M. Buil, Modelling of the corrosion of the cement paste by deionized water, Cem. Concr. Res. 22 (2–3) (1992) 489–496.
[3] C. Carde, Caractérisation et modélisation de l'altération des propriétés mechaniques due à la lixiviation des matériaux cimentaires, PhD Thesis, INSA de Toulouse, France, 1996 (in French).
[4] C. Gallé, H. Peycelon, P. Le Bescop, Effect of an accelerated chemical degradation on water permeability and pore structure of cement-based materials, Adv. Cem. Res. 16 (3) (2004) 105–114.
[5] M. Mainguy, C. Tognazzi, J.M. Torrenti, F. Adenot, Modelling of leaching in pure cement paste and mortar, Cem. Concr. Res. 30 (1) (2000) 83–90.
[6] B. Gérard, Contribution des couplages mécanique-chimie-transfert dans la tenue á long terme des ouvrages de stockage de déchets radioactifs, PhD Thesis, LMT-ENS Cachan, France, 1996 (in French).
[7] C. Le Bellégo, Couplages chimie-mécanique dans les structures en béton attaquées par l'eau: Etude expérimentale et analyse numérique, PhD Thesis, ENS Cachan, France, 2001 (in French).
[8] C. Le Bellégo, G. Pijaudier-Cabot, B. Gérard, J.F. Dubé, L. Molez, Coupled mechanical and chemical damage in calcium leached cementitious structures, J. Eng. Mech. 129 (3) (2003) 333–341.
[9] F.H. Heukamp, F.-J. Ulm, J.T. Germaine, Does calcium leaching increase ductility of cementitious materials? Evidence from direct tensile tests, J. Mater. Civ. Eng. 307 (2005).
[10] V.H. Nguyen, Couplage dégradation chimique — comportement en compression du béton, PhD Thesis, ENPC, France, 2005 (in French).
[11] E. Stora, B. Bary, Q.-C. He, E. Deville, P. Montarnal, Modelling and simulations of the chemo–mechanical behaviour of leached cement-based materials. Interactions between damage and leaching, to be submitted (2008).
[12] B. Bary, Simplified coupled chemo–mechanical modeling of cement pastes behavior subjected to combined leaching and external sulfate attack, Int. J. Num. Ana. Meth. Geomech. 32 (14) (2008) 1791.
[13] F.H. Heukamp, Chemomechanics of calcium leaching of cement-based materials at different scales: the role of CH dissolution and CSH degradation on strength and durability performance of materials and structure, PhD Thesis, Cambridge, 2002.
[14] D. Kuhl, F. Bangert, G. Meschke, Coupled chemo–mechanical deterioration of cementitious materials Part II: Numerical methods and simulations, Int. J. Solids Struct. 41 (1) (2004) 41–67.
[15] D. Kuhl, F. Bangert, G. Meschke, Coupled chemo–mechanical deterioration of cementitious materials. Part I: Modeling, Int. J. Solids Struct. 41 (1) (2004) 15–40.
[16] Y. Maltais, E. Samson, J. Marchand, Predicting the durability of Portland cement systems in aggressive environments—laboratory validation, Cem. Concr. Res. 34 (9) (2004) 1579.
[17] J. Marchand, E. Samson, Y. Maltais, J.J. Beaudoin, Theoretical analysis of the effect of weak sodium sulfate solutions on the durability of concrete, Cem. Concr. Compos. 24 (3–4) (2002) 317–329.
[18] L. De Windt, D. Pellegrini, J. van der Lee, Coupled modeling of cement/claystone interactions and radionuclide migration, J. Contam. Hydrol. 68 (3–4) (2004) 165.
[19] A. Zaoui, Matériaux hétérogènes et composites, lecture notes, Paris, Ecole Polytechnique, 1997, (in French).
[20] E. Stora, B. Bary, Q.C. He, On estimating the transport properties of hardened cement pastes, Trans. Por. Med. 73 (3) (2008) 279–295.
[21] P. Montarnal, C. Mügler, J. Colin, M. Descotes, A. Dimier, E. Jacquot, Presentation and use of a reactive transport code in porous media, Phys. Chem. Earth 32 (2007).
[22] B. Bary, S. Béjaoui, Assessment of diffusive and mechanical properties of hardened cement pastes using a multi-coated sphere assemblage model, Cem. Concr. Res. 36 (2) (2006) 245–258.
[23] G. Constantinides, F.-J. Ulm, The effect of two types of C–S–H on the elasticity of cement-based materials: results from nanoindentation and micromechanical modeling, Cem. Concr. Res. 34 (1) (2004) 67–80.
[24] V. Pensée, Q.-C. He, Generalized self-consistent estimation of the apparent isotropic elastic moduli and minimum representative volume element size of heterogeneous media, Int. J. Solids Struct. 44 (2007) 2225–2243.
[25] H.F.W. Taylor, Cement Chemistry, Thomas Telford, London, 1997.
[26] I.G. Richardson, The nature of the hydration products in hardened cement pastes, Cem. Concr. Compos. 22 (2000) 97–113.
[27] H.F.W. Taylor, C. Famy, K.L. Scrivener, Delayed ettringite formation, Cem. Concr. Res. 31 (2001) 683–693.
[28] S. Béjaoui, B. Bary, S. Nitsche, D. Chaudanson, C. Blanc, Experimental and modeling studies of the link between microstructure and effective diffusivity of cement pastes, Rev. Eur. Gén. Civ. 10 (9) (2006) 1073–1106.
[29] P.D. Tennis, H.M. Jennings, A model for two types of calcium silicate hydrate in the microstructure of Portland cement pastes, Cem. Concr. Res. 30 (6) (2000) 855–863.
[30] R.M. Christensen, K.H. Lo, Solutions for effective shear properties in 3 phase sphere and cylinder models, J. Mech. Phys. Solids 27 (4) (1979) 315–330.
[31] E. Hervé, A. Zaoui, N-layered inclusion-based micromechanical modeling, Int. J. Eng. Sci. 31 (1) (1993) 1–10.
[32] E. Stora, Q.C. He, B. Bary, Influence of inclusion shapes on the effective linear elastic properties of hardened cement pastes, Cem. Concr. Res. 36 (7) (2006) 1330–1344.
[33] Q.S. Zheng, D.X. Du, An explicit and universally applicable estimate for the effective properties of multiphase composites which accounts for inclusion distribution, J. Mech. Phys. Solids 49 (11) (2001) 2765–2788.
[34] Z. Hashin, P.J.M. Monteiro, An inverse method to determine the elastic properties of the interphase between the aggregate and the cement paste, Cem. Concr. Res. 32 (8) (2002) 1291–1300.
[35] S. Caré, E. Hervé, Application of a n-phase model to the diffusion coefficient of chloride in mortar, Trans. Por. Med. 56 (2) (2004) 119–135.
[36] M.P. Lutz, R.W. Zimmerman, Effect of an inhomogeneous interphase zone on the bulk modulus and conductivity of a particulate composite, Int. J. Solids Struct. 42 (2) (2005) 429.
[37] Z. Sun, E.J. Garboczi, S.P. Shah, Modeling the elastic properties of concrete composites: experiment, differential effective medium theory, and numerical simulation, Cem. Concr. Compos. 29 (1) (2007) 22–38.

[38] E. Stora, Multi-scale modelling and simulations of the chemo–mechanical behavior of degraded materials, PhD Thesis, University of Paris-Est Marne-la-Vallée, 2007.
[39] S. Torquato, Random Heterogeneous Materials, Springer, New-York, 2001.
[40] P. Ponte Castaneda, J.R. Willis, The effect of spatial distribution on the effective behavior of composite materials and cracked media, J. Mech. Phys. Solids 43 (12) (1995) 1919–1951.
[41] S. Igarashi, M. Kawamura, A. Watanabe, Analysis of cement pastes and mortars by a combination of backscatter-based SEM image analysis and calculations based on the Powers model, Cem. Concr. Compos. 26 (8) (2004) 977–985.
[42] P.J.M. Monteiro, C.P. Ostertag, Analysis of the aggregate-cement paste interface using grazing incidence X-ray scattering, Cem. Concr. Res. 19 (6) (1989) 987–988.
[43] C. Richet, M. Pin, F. Adenot, J. Maury, J.P. Lalle, C. Fockedey, Amélioration de la fiabilité du modèle DIFFUZON, NT SESD 97.37, 1997, (in French).
[44] B. Bourdette, Durabilité du mortier, prise en compte des auréoles de transition dans la caractérisation et la modélisation des processus physiques et chimiques d'altération, PhD Thesis, INSA de Toulouse, France, 1994 (in French).
[45] J. van der Lee, L. de Windt, Chess tutorial and Cookbook, updated for version 3.0, in: (Eds), ENSMP-CIG LHM/RD/02/13, 2002.
[46] M. Moranville, S. Kamali, E. Guillon, Physicochemical equilibria of cement-based materials in aggressive environments–experiment and modeling, Cem. Concr. Res. 34 (9) (2004) 1569–1578.
[47] D. Planel, Les effets couplés de la précipitation d'espèces secondaires sur le comportement mécanique et la dégradation chimique des Bétons, PhD thesis, Université de Marne la Vallée, 2002 (in French).
[48] G.T. Yeh, V.S. Tripathi, A critical evaluation of recent developments in hydrogeochimical transport models of reactive multichemical components, Water Resour. Res. 25 (1) (1989) 93–108.
[49] E. Nozourtier-Mazauric, Prise en compte des variations de porosité dans le couplage transport-chimie mis en œuvre dans ALLIANCES, SFME/MTMS/RT/04/016/A, technical report CEA, 2004 (in French).
[50] E. Stora, Q.C. He, B. Bary, A mixed composite spheres assemblage model for the transport properties of random heterogeneous materials with high contrasts, J. Appl. Phys. 100 (8) (2006) 084910.
[51] V. Baroghel-Bouny, Caractérisation des pâtes de ciment et des bétons. Méthodes, analyse et interprétations, PhD thesis, LCPC, 1994 (in French).
[52] C. Gallé, Effect of drying on cement-based materials pore structure as identified by mercury intrusion porosimetry: a comparative study between oven-, vacuum-, and freeze-drying, Cem. Concr. Res. 31 (10) (2001) 1467–1477.
[53] C. Tognazzi, Couplage fissuration-dégradation chimique dans les matériaux cimentaires: caractérisation et modélisation, PhD Thesis, INSA Toulouse, 1998 (in French).
[54] S. Béjaoui, B. Bary, Modeling of the link between microstructure and effective diffusivity of cement pastes using a simplified composite model, Cem. Concr. Res. 37 (3) (2007) 469–480.
[55] P.J.M. Monteiro, C.T. Chang, The elastic-moduli of calcium hydroxide, Cem. Concr. Res. 25 (8) (1995) 1605–1609.
[56] A. Boumiz, D. Sorrentino, C. Vernet, F. Cohen Tenoudji, Modelling the development of the elastic moduli as a function of the degree of hydration of cement pastes and mortars, in: A. Nonat (Ed.), Proceedings 13 of the 2nd RILEM Workshop on Hydration and Setting, France, Dijon, 1997.
[57] S. Kamali, Comportement et simulation des matériaux cimentaires en environnements agressifs: lixiviation et température, PhD Thesis, LMT-ENS de Cachan, France, 2003 (in French); S. Kamali, M. Moranville, E. J. Garboczi, S. Prené, B. Gérard, Hydrate dissolution influence on the Young modulus of cement pastes, proceedings of the 5th international conference on fracture mechanics of concrete and concrete structures (FRAMCOS V), in: Li et al. (Eds.), Vail, USA, 2 (2004) 631–638.
[58] B. Bary, Simulation de la carbonatation des matériaux cimentaires de la barrière ouvragée ANDRA en conditions insaturées, NT DPC/SCCME 05-702-A, 2005, (in French).
[59] K. Scrivener, Backscattered electron imaging of cementitious microstructures: understanding and quantification, Cem. Concr. Compos. 26 (8) (2004) 935–945.
[60] H.M. Jennings, J.J. Thomas, J.S. Gevrenov, G. Constantinides, F.-J. Ulm, A multi-technique investigation of the nanoporosity of cement paste, Cem. Concr. Res. 37 (3) (2007) 329.
[61] J. Sanahuja, L. Dormieux, G. Chanvillard, Modelling elasticity of a hydrating cement paste, Cem. Concr. Res. 37 (10) (2007) 1427–1439.
[62] C.J. Haecker, E.J. Garboczi, J.W. Bullard, R.B. Bohn, Z. Sun, S.P. Shah, T. Voigt, Modeling the linear elastic properties of Portland cement paste, Cem. Concr. Res. 35 (10) (2005) 1948–1960.
[63] G. Constantinides, F.-J. Ulm, The nanogranular nature of C–S–H, J. Mech. Phys. Solids 55 (1) (2007) 64–90.